Version 2.1 - June 9, 2001
Note LHCb 2001-027 Muon

Design and Construction of the RPC Detector for the LHCb Muon system

A. Bizzeti [a], M. Calvetti [a], G. Carboni [b], G. Collazuol [a], S. De Capua [b], D. Domenici [b], G. Ganis [b], M. Gatta [b], R. Messi [b], L. Paoluzi [b], G. Passaleva [a], E. Santovetti [b], M. Veltri [a]

[a] *Università di Firenze and INFN, Firenze, Italy*
[b] *Università degli Studi di Roma "Tor Vergata" and INFN, Roma, Italy*

June 9, 2001

Abstract

We present the design of the RPC detectors for the LHCb Muon system and the present ideas about construction and assembly phases. We give an updated estimate of the costs.

Contents

1 Introduction

In our previous note [1] we presented a proposal for equipping the outer region of the LHCb muon detector with Resistive Plate Chambers (RPC). A baseline solution with RPCs in regions 3 and 4 of muon stations 4 and 5 has been chosen by the collaboration [2]. The main purpose of this note is to present a detailed design of the RPC detectors for LHCb to support the Technical Design Report for the Muon System [3]. Some of the needed information has been extracted from tests performed after the submission of the proposal; this is discussed in the next section. We also present more detailed considerations about construction and assembly phases, and an updated estimate of the costs.

2 Updated tests of prototype performances

In this section we describe further tests that have been done on prototypes to answer to the main questions left open in Ref. [1]. These concern the choice of a baseline solution for the front-end electronics and the possibility of reading out the chambers with wider pick-up strips.

2.1 Front-End electronics

In Ref. [1] we presented two possibilities for the readout chip: the GaAs based solution adopted by ATLAS and the BiCMOS based chip developed by CMS. Unfortunately the production process on which the former solution was based became in the meanwhile obsolete, ruling out such a possibility. A few BiCMOS chips were kindly made available to us by the CMS-Bari group.

2.1.1 The BiCMOS front-end chip

The properties of the CMS readout chip [4] are summarized in Table 1. The front-end CMS ASIC chip has been designed and manufactured in the 0.8 μm BiCMOS technology. The circuit comprises eight channels, each consisting of an amplifier, a zero-crossing discriminator, a mono-stable and a differential LVDS line driver. A block diagram for the single channel is shown in Figure 1. The preamplifier has an input impedance of about 15 Ω at the signal frequencies. Such a low value for the input impedance has been chosen to match the lowest value of the characteristic impedance of the CMS strips, and is close to the characteristic impedance of our 6 cm wide strips (13 Ω).

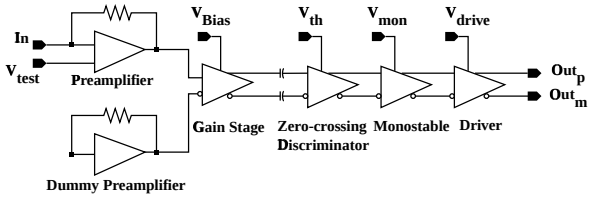

Figure 1 Single-channel block diagram for the CMS front-end chip [4].

Table 1 Nominal properties of the CMS readout chip.

Technology	0.8 μm BiCMOS
Dimensions	2.9×2.6 mm^2
Input Impedance	$\sim$15 Ω
Input Polarity	negative
Dynamic Range	20 fC – 20 pC
Threshold Range	20 fC – 500 fC
Charge Sensitivity	$\sim$1 mV/fC
Preamp Bandwidth	116 MHz
Equivalent Noise Charge	4 fC
Output pulse width	50 ns – 300 ns
Output level	LVDS
Power supply	+5 V, GND
Power consumption	$\sim$45 mW/channel

2.1.2 Calibration and test

Test and calibration of the chips, mounted on the first version of the Front-End Board (see Section 3.4), have been performed as follows. The channel under test has been fed with a signal of variable amplitude $V_{\rm in}$ through a capacitor of $C_{\rm in}$=1.8 pF connected directly to the input terminal on the FEB. Measuring the efficiency of the chip to produce a signal as a function of $V_{\rm in}$ allows the determination of the effective threshold $V_{\rm eff}$, corresponding to the charge $V_{\rm eff} \cdot C_{\rm in}$. We have also measured the arrival time of the chip response with respect to a trigger signal also provided by the generator of the test pulse; in this way the jitter of the chip response could be measured.

A typical result for threshold determination is shown in Figure 2, top: the slope at the point where the efficiency crosses 0.5 is a measure of the amplifier noise which is of the order of 2 fC, in agreement with the specifications from the Bari group.

The average threshold calibration over the eight channels of one of the tested chips is shown in Figure 3, top-left, as a function of the nominal threshold value. The minimum/maximum variation at each point are shown as error bars, giving visually an idea of the uniformity within the chip. This is given quantitatively in the middle part of the figure, where the RMS of the eight channels is shown for the effective threshold determinations; the spread over the chip is of the order of 5% of the mean value.

The bottom-left plot in Figure 2 shows a typical result for the measured jitter, the RMS of which is of the order of 0.15 ns. The RMS of mean jitter as a function of the nominal threshold is shown in Figure 3, bottom-left. The uniformity is within 0.35 ns, which is negligible when compared to the time resolution of the system. The three plots on the right of Figure 3 show the uniformity among the six chips tested insofar.

For the future we plan to automatize and speed-up the test procedure using a readout system which should allow to test a significant sampled fraction of the total amount of chips.

2.1.3 Radiation hardness

The $0.8\,\mu$m BiCMOS technology is not intrinsically radiation hard. However, the radiation doses expected during operation of the LHCb detector are relatively small: about 10 Gy/year.

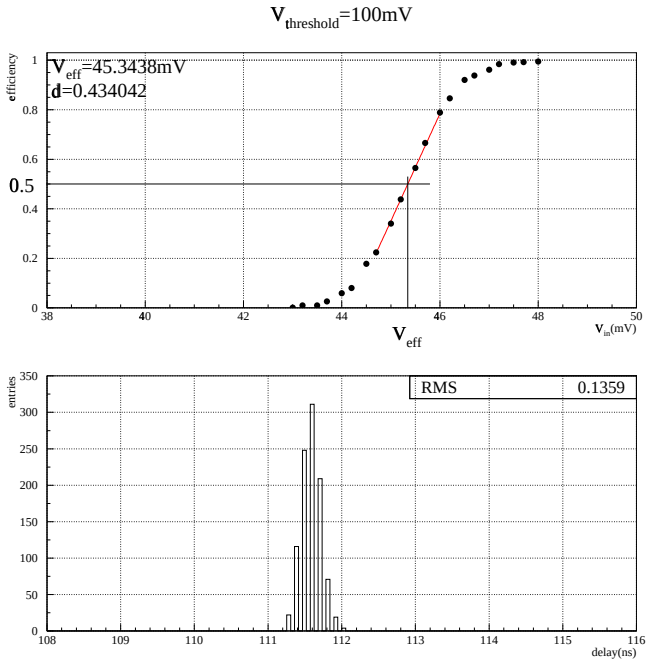

Figure 2 Example of result from chip calibration at a nominal threshold of 100 mV. *Top*: efficiency as a function of the input signal defining V_{eff}. *Bottom*: arrival time of the chip response.

The CMS collaboration has performed a test using photons (1.7 Gy) and fast neutrons (70 Gy equivalent) and found no performance modification [5].

2.2 Testbeam measurements

2.2.1 RPC with BiCMOS electronics

The BiCMOS chip has been designed to read out the double-gap RPC chambers of the CMS experiment. The CMS chambers differ from the ones proposed for LHCb in terms of the layout of the readout plane and the composition of the gas mixture (no SF_6 in CMS). To assess if the BiCMOS chip is suited for our needs, we have measured the efficiency and cluster size of a real RPC chamber read out with BiCMOS electronics in the X5 beam facility. For this purpose we equipped a 50×50 cm^2 single gap RPC with 16 channels, reading the signals picked-up on 16 strips of dimensions 3×25 cm^2. These strips were terminated according to their characteristic impedance of about 27Ω. This RPC is referred hereafter as "BiCMOS RPC". As a reference we also measured in the same conditions a RPC of the same size equipped with the so called "standard" electronics used for our previous tests. The strip length on this reference RPC was 50 cm. For practical reasons the effective thresholds were different: about 120 fC on the reference RPC, about 180 fC for the CMS electronics.

The results of the test are shown in Figure 4. The top plot shows the efficiency as a function of the applied voltage; the plateau starts at higher voltages for the BiCMOS RPC because of the higher threshold. The middle plot shows the relation between cluster size and efficiency, which is not expected to depend on the threshold value. Finally the bottom plot shows the cluster size as function of the position where the particle crosses the strip. Here we see that the BiCMOS RPC has smaller direct cross talk (the peaks near the strip borders are narrower)

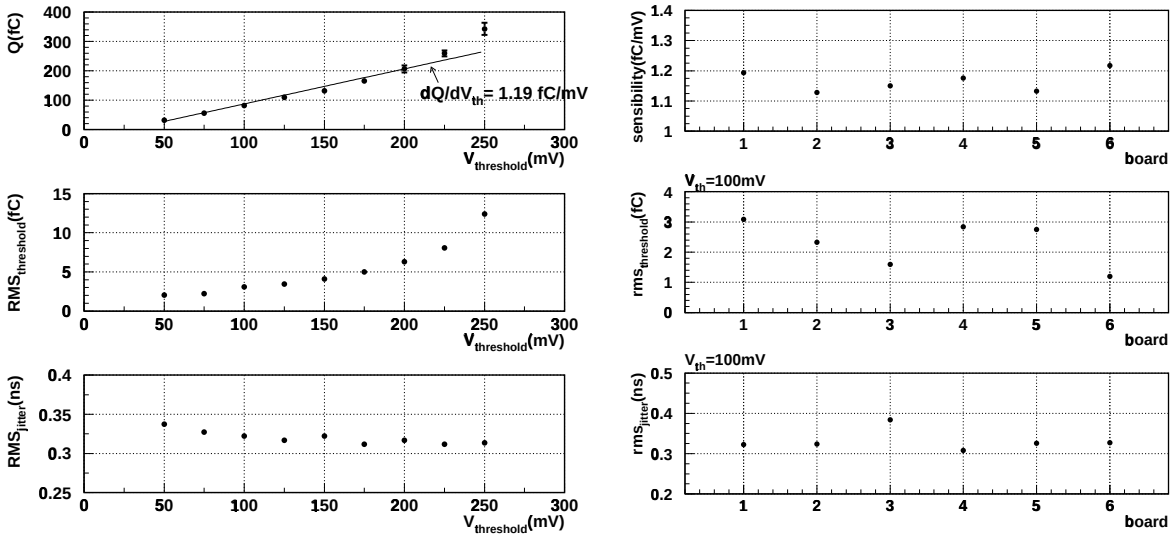

Figure 3 Test of a front-end chip (left column): average effective charge as a function of the nominal threshold (top; the error bars indicate the range of variation of the eight channels); RMS of the results of the eight channels (middle); RMS of the mean arrival times of the eight channels (bottom). Summary results for the six BiCMOS chips calibrated (right column): calibration slope (top); slope RMS for a threshold of 100 mV (middle); jitter RMS (bottom).

as expected from a higher threshold. On the contrary, the capacitive cross talk, measured in the middle of the strips, is similar, whereas one would expect it smaller for the BiCMOS RPC because of the shorter strips; we have not studied this in detail, but the qualitative explanation is based on the fact that the capacitive cross talk also depends on the peaking time and it is expected to be larger for the faster electronics [6], which in this case is the CMS one. The small differences between the two sets of results can therefore be understood with the differences in the applied thresholds and in the electronics timing properties.

From this test we can draw the conclusion that the CMS BiCMOS electronics satisfies our basic requirements and, therefore, can be chosen as baseline for the RPC readout. Depending on the availability, we plan to test also the ASDQ [7] and CARIOCA [8] chips developed for the MWPC, which potentially have some nice feature that could allow operation of RPCs at lower threshold.

2.2.2 Test of a RPC with 6 cm strips

The measurements described in [1] and in the previous section have all been done using 3 cm wide strips to read out the detectors. The possibility to reduce the number of readout channels by doubling the strip width has been envisaged and taken as baseline solution ([3], Table 1). Tests of the detector performance with 6 cm wide strips were therefore needed. For this purpose a 50×50 cm^2 single–gap RPC, oiled [1], was equipped with 30 cm long readout strips, terminated on their characteristic impedance, which is about 13 Ω, i.e. half the one of the 3 cm wide strips. The signals induced on the strips were read out with the BiCMOS electronics. A

[1]The standard ATLAS linseed oil treatment (oil:eptane = 40:60) was applied.

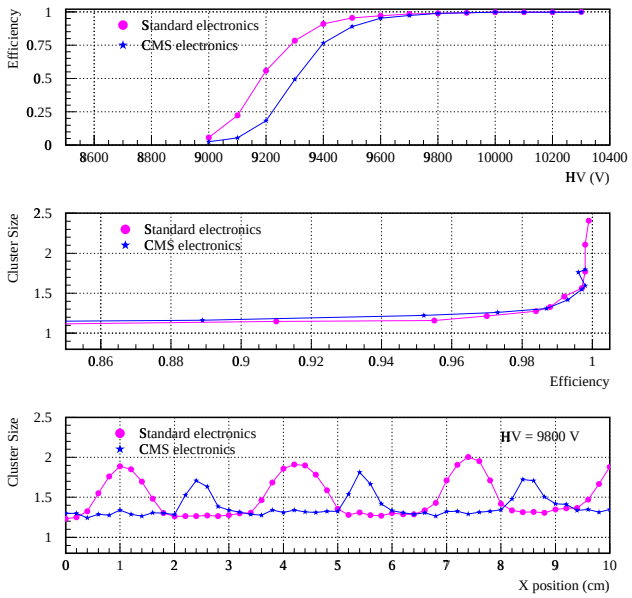

Figure 4 Comparison between the performances of two identical chambers equipped with "standard" and CMS electronics: Efficiency vs applied voltage (top); Efficiency vs Cluster Size (middle), Cluster Size vs X strip position (bottom); strip size was 30 mm for this test.

scintillator telescope was setup in the laboratory as shown in Figure 5. The selected area was about 6×6 cm^2.

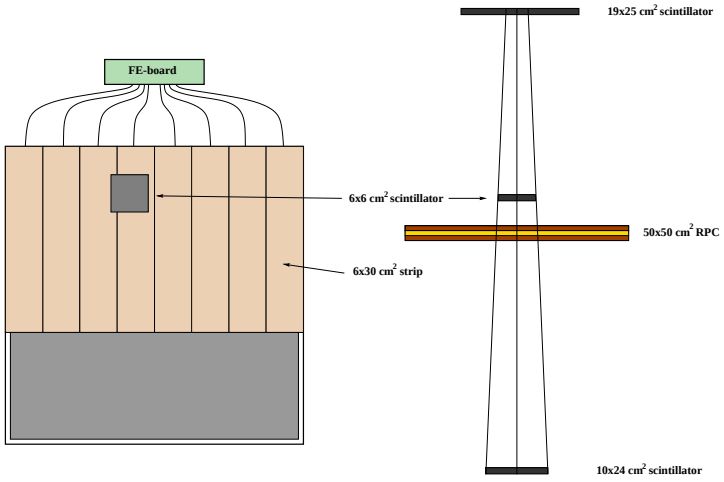

Figure 5 RPC with 6 cm readout strips: laboratory setup for tests with cosmic rays.

As shown in Figure 6, left, the time resolution remained better than 1.2 ns, therefore not worsened by the use of the new electronics and the new strip size. Figure 6, right, shows the dark noise rate per channel which was always less than 0.2 Hz/ cm^2.

Figure 7 shows the efficiency curve for two threshold values of about 70 fC, 100 fC and 130 fC; the efficiency in the plateau was larger than 97% in all cases. The cluster size over the

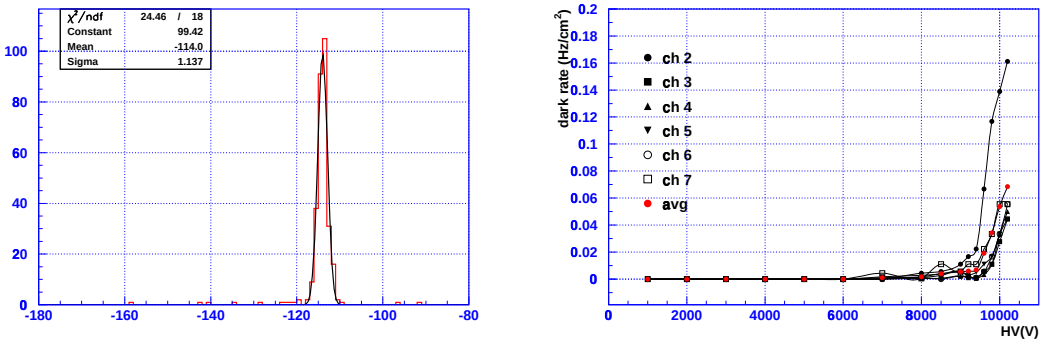

Figure 6 RPC with 6 cm readout strips. *Left*: time resolution with BiCMOS electronics (trigger resolution unfolded). *Right:* dark rates as a function of the applied voltage for the readout channels.

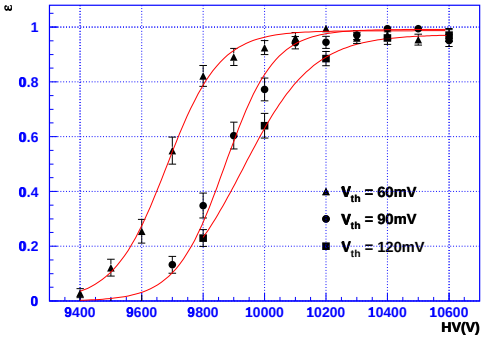

Figure 7 Cosmic rays test of a single-gap RPC readout with 6 cm wide strips and BiCMOS electronics: Efficiency vs. applied voltage for three different threshold values.

beam spot, *i.e.* essentially over one strip, has also been measured. An example is shown in Figure 8, left. In Figure 8, right, the measured efficiency is shown as a function of the average cluster size for two values of the threshold. For comparison, the range of values obtained with 3 cm wide strips in the test beam measurement reported in the previous section are also shown. We see that with wider strips the performances in terms of cluster size are very satisfactory and close to the very best case which could be obtained with 3 cm wide strips. However, a precise assessment of the capacitive and geometrical contributions to the cluster size needs further measurements with test beams, scheduled for the near future.

3 RPC detectors

3.1 System overview

A schematic overview of the RPC system is given in Figure 9. Part of the readout chain (the Intermediate–Boards and the Off–Detector–Boards) is in common with the rest of the muon system. All the other components shown in the figure are specific or have specific requirements

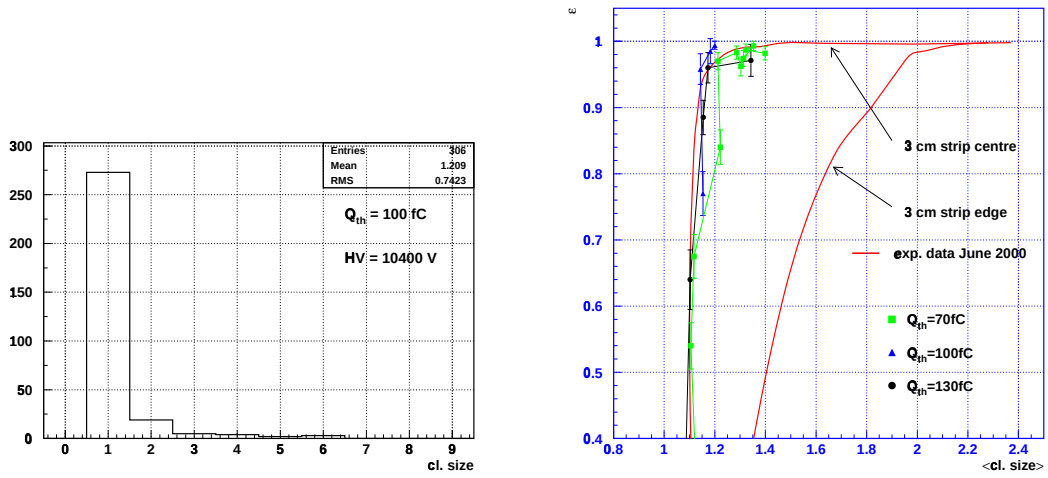

Figure 8 Cosmic rays test of a single-gap RPC readout with 6 cm wide strips and BiCMOS electronics. *Left*: example of cluster size at full efficiency. *Right*: Cluster Size vs. Efficiency for three different threshold values. The thin (red) lines are the measured curves for a a similar chamber readout with 3 cm wide strips in the two extreme conditions corresponding to particles crossing at the strip centre and in between two strips.

from the RPCs. These will be discussed in the next subsections.

3.2 Detector overview

The choice of the type of RPC detector is driven by efficiency and redundancy considerations of the system requiring two independent measurements of the traversing particle per each muon station. This leads to a configuration with two detectors per station. We have shown in Ref. [1] that the OR of two single gap RPC satisfies the requirements of having a good efficiency plateau for an average cluster size below 2. Therefore, we have chosen as baseline the configuration shown schematically in Figure 10. The two strip planes, read out independently, are placed between the two gas gaps in such a way to provide automatically the shielding of the two gaps. The graphite ground layer faces the readout plane, a configuration which reduces the pickup of power supply noise.

3.2.1 Chamber design

The chamber physical dimensions are determined by the logical pad sizes and the attempt to minimize the number of chamber types. All the relevant numbers are summarized in Tables 1 and 2, and visually represented in Figure 11. The optimization of the Muon system logical layout [9], has led, for station 4 (5), to logical pad sizes of 116×145 mm^2 (124×155 mm^2) in region 3 and of 232×290 mm^2 (248×309 mm^2) in region 4. The minimal number of chamber types per station is then obtained with chamber sizes with active area of 1391×290 mm^2 and 1485×309 mm^2 in station 4 and 5, respectively. This solution corresponds to strips running vertically along the shortest side of the chambers. In region 4 the strips have the full length (about 300 mm) and are read out at one end. In region 3 they are cut in the middle and are

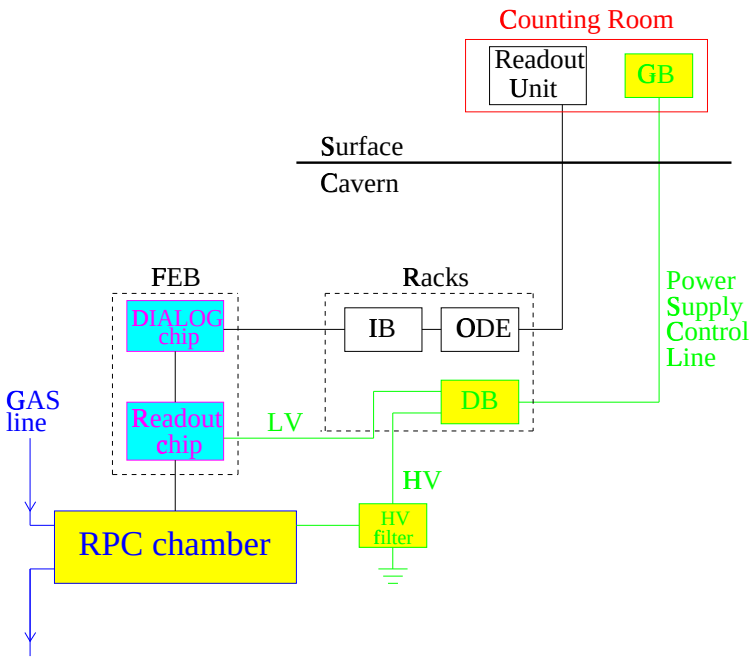

Figure 9 Schematic overview of the RPC system. Acronyms: Front–End–Boards (FEB), Intermediate–Boards (IB), Off–Detector–Boards (ODE), Power Supply Generator–Box (GB), Power Supply Distributor–Box (DB).

read out at both ends, on the chamber upper and lower edges. The baseline solution for the strip width in station 4 (5) is 56 (60) mm, located with a pitch of 58 (62) mm and interleaved with narrow ground strips of 0.5 mm. The shortness of the strips should allow operation without termination [6], which would simplify construction; however, this solution needs some additional test. Finally, in order to further simplify the construction we plan to have the same gap size for all the chambers. This is possible since the active area of the detector can be determined by the graphite paint, which can therefore be adjusted according to the needs in each station.

To summarize, the physical dimensions will be the same for all the chambers of a given station; a different strip readout is however needed for regions 3 and 4; this makes a total four different chamber types, the relevant quantities of which are summarized in Table 2.

An exploded view of the RPC chamber is shown in Figure 12.

3.2.2 Mechanical structure and design

The design of the mechanical structure is driven by the requirements of low specific weight ($<$20 kg/m^2), small overall thickness ($<$60 mm) and rigidity of the whole system.

A detailed cross section of the basic chamber is shown in Figure 13. Each RPC detector

Table 2 Relevant numbers of the LHCb muon system in the regions equipped with RPCs. Where relevant, the horizontal dimension, i.e. the one in the bending plane, is given first.

Physical quantities:	Region 3		Region 4	
	Station 4	Station 5	Station 4	Station 5
Detector Surface (m^2)	19.3	22.1	77.4	88.3
Horizontal dimension (cm)	139	149	278	297
Vertical dimension (cm)	116	124	232	248
Number of chambers	48	48	192	192
Chamber sensitive area (cm^2)	139×29	148.5×30.9	139×29	148.5×30.9
Channel size (cm^2)	5.8×14.5	6.2×15.5	5.8×29.0	6.2×30.9
Maximal rate (Hz/cm^2)	750	650	250	190
Logical quantities:	Region 3		Region 4	
	Station 4	Station 5	Station 4	Station 5
Horiz. channel size (cm^2)	69.5×14.5	74.3×15.5	139.1×29.0	148.5×30.9
Vertical channel size (cm^2)	11.6×57.9	12.4×61.9	23.2×115.9	24.8×123.8
Pad granularity (cm^2)	11.6×14.5	12.4×15.5	23.2×29.0	24.8×30.9
Number of horizontal strips	48	48	48	48
Number of vertical strips	72	72	72	72
Number of logical channels	120	120	120	120

Table 3 Relevant numbers for the four RPC chamber types.

Type	Region	Station	Number	Sensitive area X×Y (cm^2)	Strip size X×Y (cm^2)	Number of physical channels
4.3	3	4	48	139×29	5.8×14.5	48×2
5.3	3	5	48	148.5×30.9	6.2×15.5	48×2
4.4	4	4	192	139×29	5.8×29.0	24×2
5.4	4	5	192	148.5×30.9	6.2×30.9	24×2
Total:			480			27648

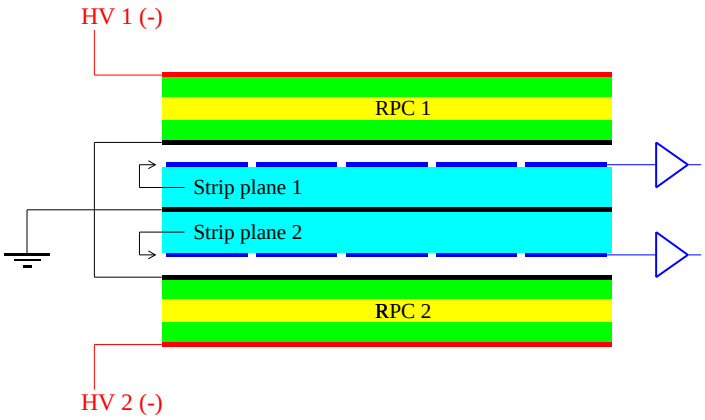

Figure 10 Schematic layout of the chamber with two independent RPC showing the two gaps (RPC 1 and RPC 2) and the readout strip assembly in the middle.

(Figure 14) is made of two bakelite plates 2 mm thick; the choice of the bakelite volume resistivity is driven by considerations about rate capability; we plan to use bakelite with volume resistivity of $(6–10)\cdot 10^9$ Ωcm. The bakelite is laminated with a thin melamine layer on the side facing the gas, with the purpose of reducing the noise by improving on the quality of the surface [10]. The bakelite plates are kept parallel by polycarbonate spacers, 10 mm in diameter, and 2.00 ± 0.01 mm in height, positioned to form a square array of 10×10 cm^2 basic unit. The topology for spacer positioning is different in the two RPCs of a chamber to avoid correlated blind zones. A polycarbonate rectangular frame, 7 mm wide and of the same height and tolerances of the spacers, is used to close the gap on the edges. The spacers and the frame are visible in Figure 13. The circulation of the gas is insured by four gas inlets/outlets placed at the four corners of the detector. They are also made of polycarbonate and are 3 mm in diameter. All these parts (bakelite plates, spacers, frame, gas in-out/lets) are glued together using epoxy adhesives. Externally to the gaps, the graphite layers will have a surface resistivity of about 100 kΩ/square and are electrically insulated by means of 200 μm thick Polyethylene-Teraphtalate (PET) films glued on the graphite itself (Figure 14).

The mechanical rigidity of the chamber will be insured by an external aluminum case as shown in Figure 13. The two external panels are made of a light material, like expanded polystyrene [2], 40 kg/m^3 density, sandwiched between two aluminum sheets, 0.5 mm thick, glued with epoxy adhesives. The overall thickness of each panel will be of about 10 mm. These panels are rigidly connected on the sides by shaped aluminum profiles, 2 mm thick, as also shown in Figure 13. The right pressure on the detector gaps is insured by polycarbonate spacers placed in between the gaps and the external panels in correspondence of the internal spacers.

[2]We should mention here that according to the report *Safety Instructions 41*, polystyrene is not suited for use in LHC experiments. Alternative materials are under investigation.

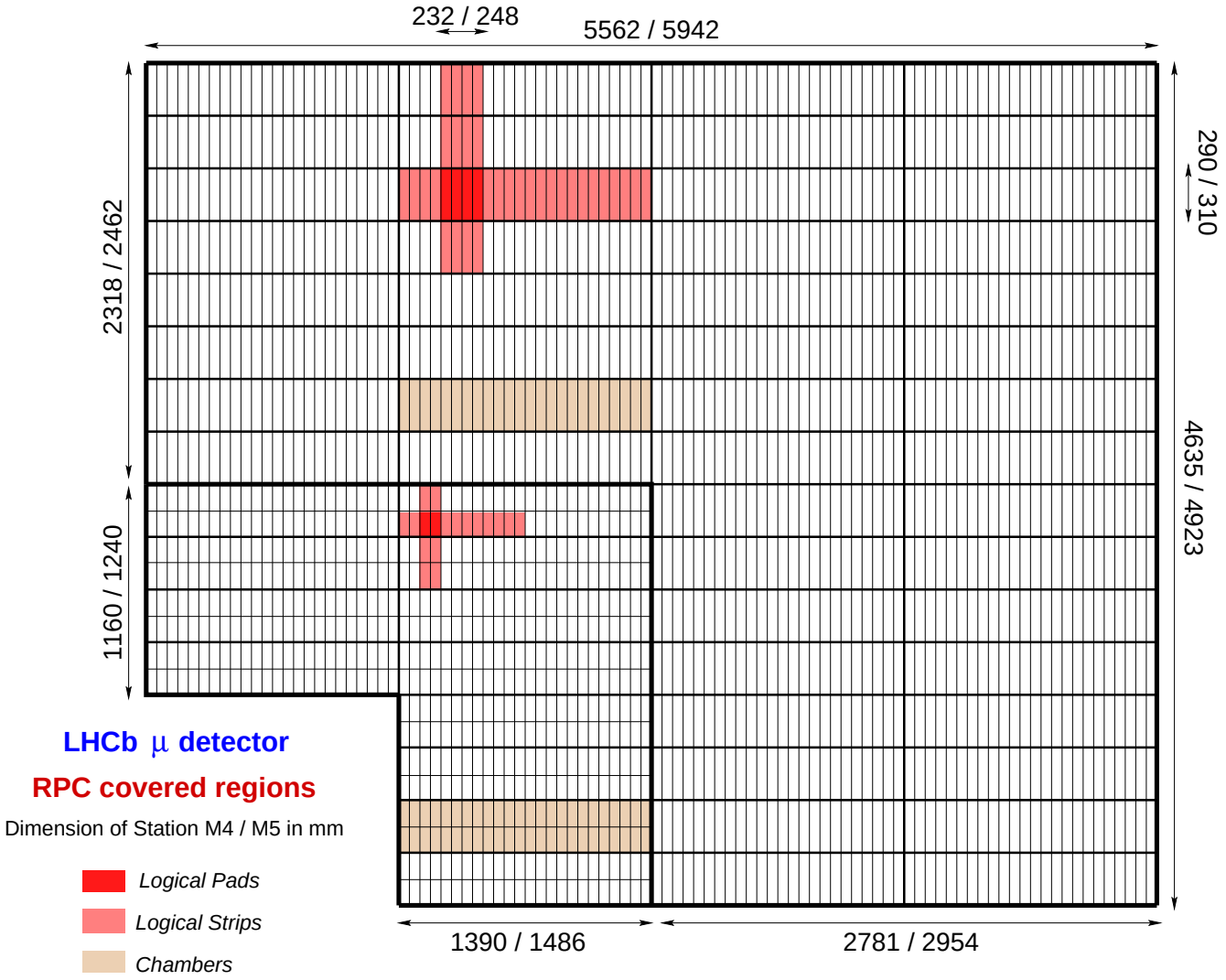

Figure 11 Definition of the relevant basic units in the station layout. The dimension of the logical strips in region 3 are half of those quoted for region 4.

3.2.3 Signal readout

As mentioned above the strip planes are located close to the center of the whole system, with their ground planes facing each other. Figure 15 shows an enlarged cross section of the strip planes. To improve the modularity of the system and to simplify the construction we plan to connect the signal strips and the front-end electronics via a standard connector as shown in Figure 13. In this way the signal generation part of the chamber is electrically insulated from the rest, a configuration which minimizes and stabilizes the noise of the chambers. We are considering the feasibility (in terms of cost and dielectric properties) of printing the strip/micro-strip configuration on a FR4 layer, 0.8 mm thick, which would then be glued on a 3.2 mm thick plate made of an expanded foam–like material. The basic strip modules will look as in Figure 16; this solution would additionally simplify the construction by avoiding the use of interconnecting cables for the extraction of the signal.

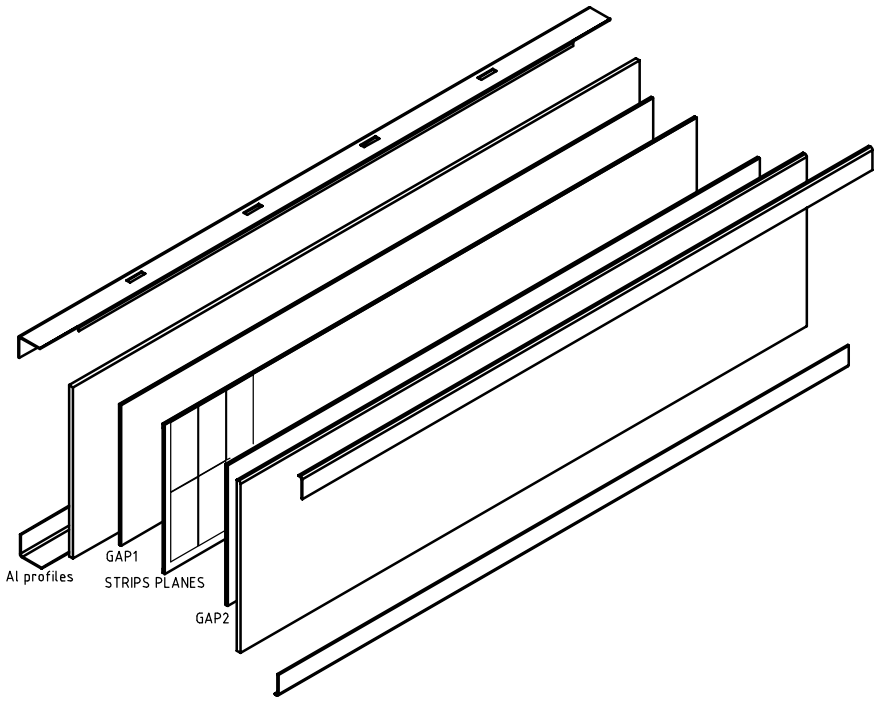

Figure 12 Exploded view of the RPC chamber.

3.2.4 Integration in the LHCb muon detector

The choice of having the same physical dimensions for MWPCs and RPCs has simplified the integration of the basic chamber in the each muon station. The relevant requirements about specific weight and overall thickness of the chambers are satisfied by the choices described in the previous sections, and prototype solutions for the overall integration avoiding dead spaces and with the necessary space for cables and gas pipes have already been presented by the Frascati and CERN groups [11].

3.2.5 Thermal considerations

The main source of power dissipation of the RPC system is the Front-End electronics: the 96 channels reading out the chambers in region 3 will dissipate about 4 W, equivalent to 8 W/m^2. This may require some cooling system; some tests of possible solutions are planned. Furthermore, the power dissipation in the RPC detector itself is not *a priori* entirely negligible. Assuming an average particle flux of $\dot{\Phi}_0 = 375\,\mathrm{Hz}/\,\mathrm{cm}^2$ (Region 3), the current density turns out to be $J' \simeq 10\ \mathrm{nA}/\,\mathrm{cm}^2$ or $100\ \mu\mathrm{A}/\,\mathrm{m}^2$. At 10 kV the power $\mathcal{P}$ dissipated in the gas of the RPC gap is about 1 W/m^2.

The temperature rise of the system due to the dissipation of $\mathcal{P}$ can be estimated as follows. Under the assumption that the molar specific heat is $c_p = 4R$, the temperature rise of the gas per second is given by

$$\dot{\mathcal{T}} = \frac{\mathcal{P}}{\mathrm{n4R}} \simeq 0.3\ \mathrm{K/s}$$

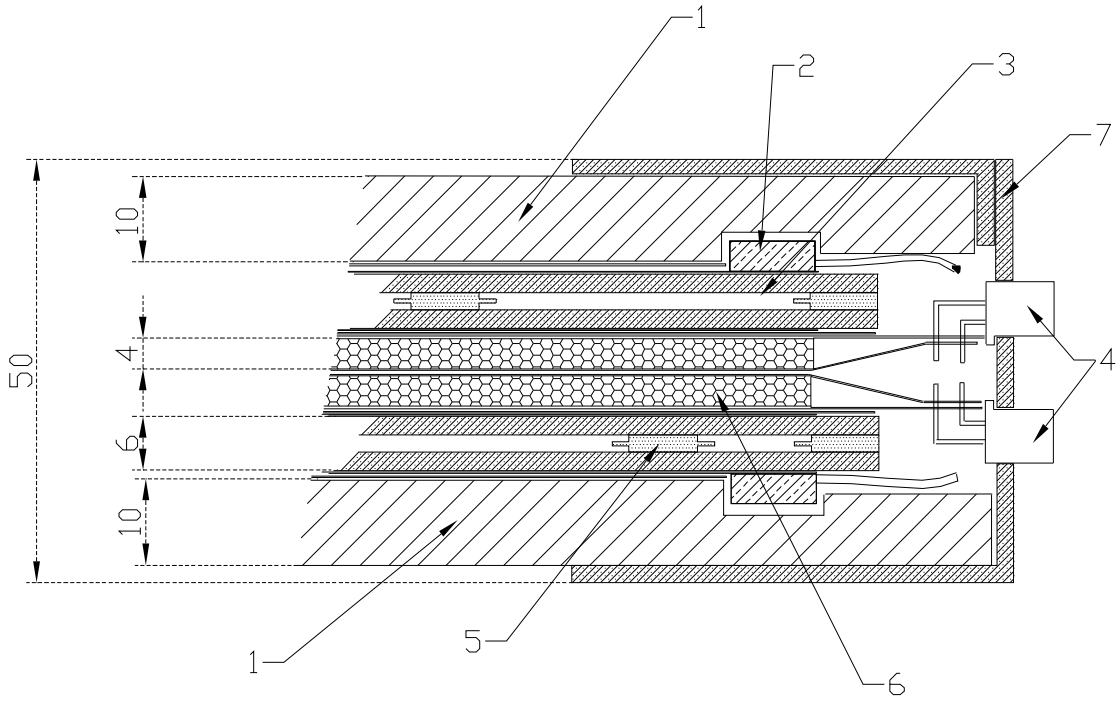

Figure 13 Chamber cross section: Al-polystyrene external panels (1); HV contacts (2); RPC detectors (3); 3M connectors (4); polycarbonate spacers (5); strip planes (6); shaped-aluminum external profiles (7). Dimensions are in mm.

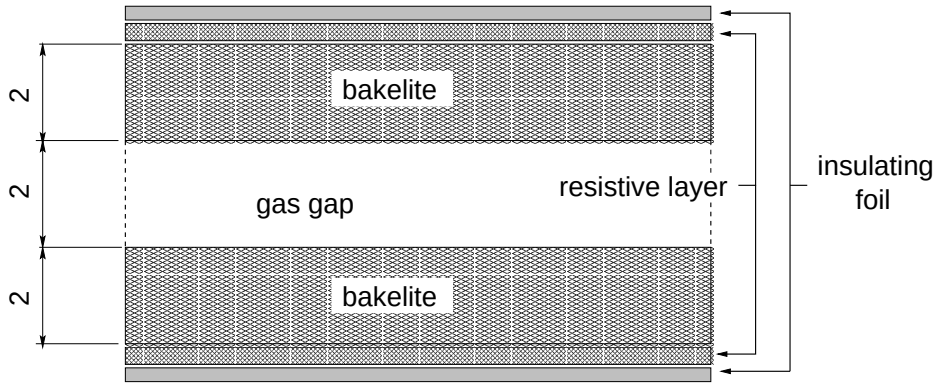

Figure 14 RPC detector cross section. The insulating foil and the resistive layers are not to scale. Dimensions are in mm.

(here $n \simeq 0.01$ is the number of moles). Therefore the gas will rapidly go to thermal equilibrium with the bakelite and the surrounding structure. Taking into account the thermal conductivity of the bakelite (κ_b=0.2 W/(m K)) and of the expanded foam layers (κ_p=0.029–0.042 W/(m K)) we obtain for the temperature rise of the detectors

$$\Delta T(^oC) \simeq \mathcal{P}\frac{d}{\kappa_p} \simeq 0.34\ ^oC,$$

d being the thicknes of the bakelite layer. Therefore, even in the most pessimistic hypothesis

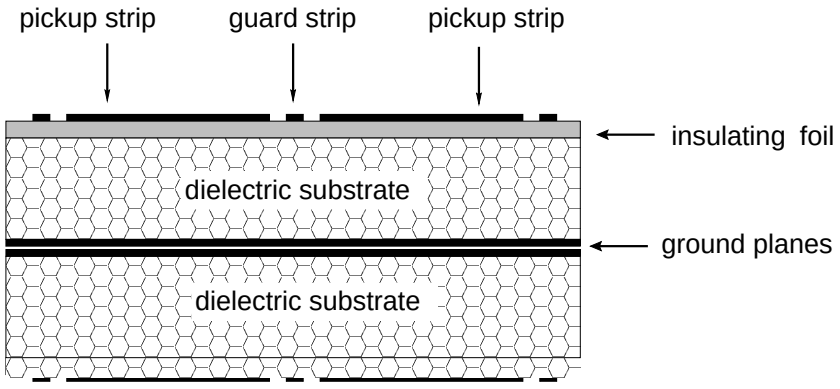

Figure 15 Cross section of the strip planes.

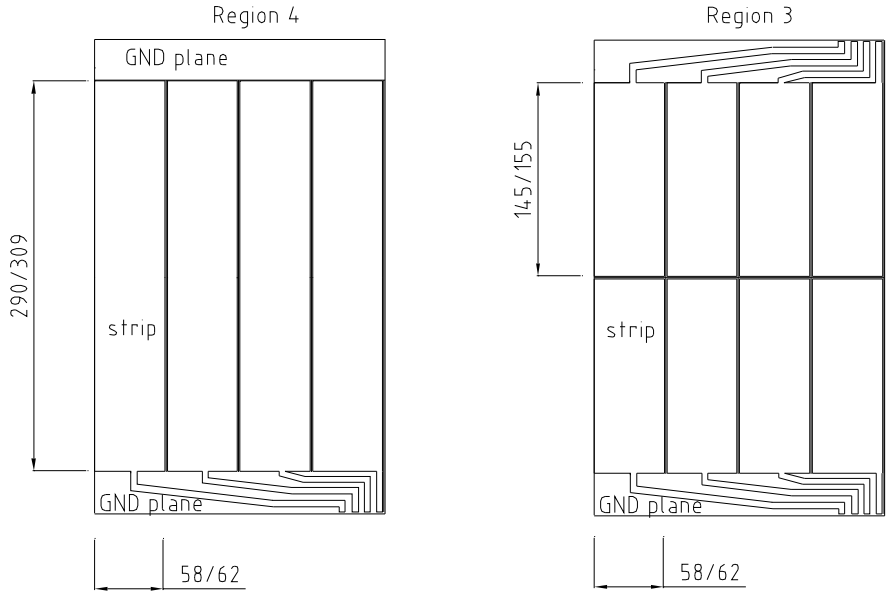

Figure 16 Printed circuit for strip planes.

that the heat is dissipated by convection only, the rise of the system temperature is rather modest [3].

3.3 Considerations about linseed oil treatment

It is well known that depositing a thin layer of linseed oil on the bakelite surface has the effect of improving the characteristics of the surface, and helps in reducing the noise and the dark current of the RPC. This happens partly because linseed oil has a larger conductivity than the bakelite.

[3] We have cross-checked this with the help of the calculator provided in Ref. [12].

The treatment of the bakelite plates with linseed oil was recently much debated in the RPC community. This was triggered by the problems faced by BABAR [13], which were attributed to high-temperature operation coupled with improper oil polymerization: in a "sticky" layer the oil can form "stalagmites" because of electrostatic attraction, that can eventually short-circuit the gap making the RPC stop working.

Since the oil is applied when the gap is assembled and sealed, quality control of the layer is very difficult. Therefore it would be preferable to avoid the oil treatment, which would also simplify the construction of the detectors. However, this will unavoidably increase both dark currents and noise.

The increased dark current will result in extra ageing. In order to control this effect, the dark current should be kept below the current due to the flux of real particles traversing the detector (see Table 2). Considering as acceptable an extra-ageing of 25% (referred to chambers in Region 3), RPCs without oil treatment will be considered a viable solution if the dark current density can be kept below 3 nA/ cm^2 or 30 μA/ m^2. Assuming that the average charge of the noise hits is 30 pC this corresponds to a maximum noise rate of 100 Hz/ cm^2 per RPC gap, which is well below the rate acceptable by the trigger (see Figure 17).

Preliminary studies performed by the CMS collaboration with non-oiled chambers [14] have shown that with the melamine treatment of the bakelite plates it is possible to reach full efficiency keeping the noise level below 50 Hz/ cm^2.

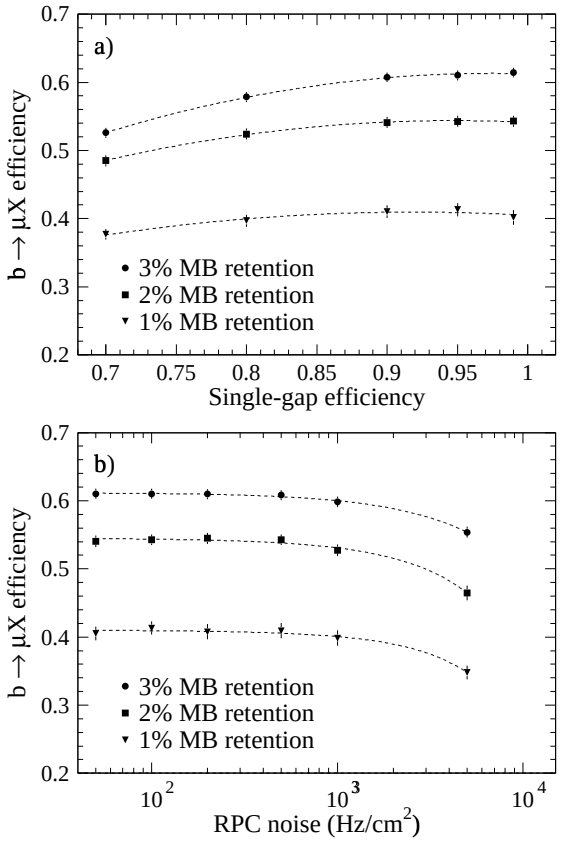

Figure 17 Effect of lowering of single gap efficiency (top) and RPC noise (bottom) on trigger performance. Three values of minimum-bias retention are considered.

A test of RPCs without linseed oil treatment is planned, in order to assess if these detectors

can be used in the experiment.

3.4 Front-End Board

The purpose of Front-End Board (FEB) is to house the electronics that produces the signals for high level processing. The FEBs will be directly plugged on the detector side being readout.

The structure of the FEBs has not yet been frozen. The Front-End architecture [15] requires that part of the logic states are moved on the detector. For this purpose, a new chip called DIALOG (DIagnostics, time Alignment and LOGics) is being developed, the functionality of which comprises the possibility to adjust the timing of each single channel and to make different OR and, for debugging purposes, AND combinations of the input signals. At present stage the DIALOG foresees 16 LVDS inputs with four ORing or ANDing possibilities: 3×8 channels (OR8, AND8, 2 outputs), 6×4 channels (OR4, AND4, 4 outputs), 12×2 channels (OR2, AND2, 8 outputs).

The number of physical channels in the case of RPCs is 2×24 per each chamber side being read out. These channels are processed by 6 readout chips and by three DIALOG chips.

Two approaches have been considered. The first is to have two different types of boards, one for the readout chips and one for the DIALOG boards; the latter could possibly be standardized for all the chambers in the muon system. The second approach is to have only one board housing the two different types of chips. This would allow minimizing the number of output connectors. The two approaches are presently being discussed, and the choice will be taken after testing on prototypes.

The operational requirements of the CMS readout chip are a LV supply of +5V and a signal to adjust the threshold. This can be either a DAC register (three of these are presently foreseen in the DIALOG design) or via a voltage variable in the range 0–5 V. Here again the final decision will be taken after testing on prototypes. The power and threshold setting should be provided via ECS.

A first prototype of a FEB with 8 channels only has been developed for the test chambers and is shown in Figure 18; this prototype is designed to read out 8 strips 3 cm wide, with the channel inputs directly soldered on the strips, i.e. without intermediate connectors. This prototype implements the remote threshold setting via additional adjustable voltage. The second prototype, presently under development, should be close to the final form, housing two chips and the connectors to take the signal out of the chambers. This FEB will read out the 16 signals corresponding to 8 adjacent physical channels. The channels of the chips will be assigned to the readout strips in such a way that, in the event of a faulty chip, a physical channel is not completely dead.

3.5 Service systems

3.5.1 Power supply system

Power supply requirements for the RPC system are related to the high voltage (HV) to be applied to the gas gaps (maximum 12 kV) and the low voltage (LV) needed to power the FEB boards (a single positive voltage is required). The RPC system needs 960 HV and 960 LV channels.

The RPC power supply system is made of two main blocks: a main board (Generator Board, GB), located in the counting room, supplying 48 V and managing the remote con-

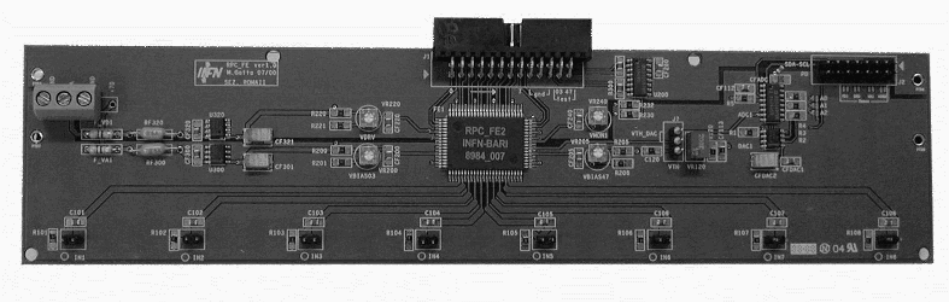

Figure 18 Picture of the first version of the Front-End Board.

trols and monitoring, and a remote system (Distributor Box, DB), located in the Off-Detector-Electronics racks, consisting of a radiation tolerant board hosting a transformation stage generating the high and the low voltages. This scheme minimizes the problem of distributing the high voltage over long distances, keeping at the same time in a safe environment the main power supply controllers which are radiation sensitive.

The GBs are able to supply 48 V, a medium voltage easy to distribute over long distances with conventional cables, and supports a communication link for remote control and monitoring purposes. The GBs are interfaced with the general LHCb DCS and are placed in the counting room allowing an easy and safe access to the power supply system.

The DBs represent transformation stages where the input 48 V are transformed into two HV channels and four LV channels. Both the HV and the LV channels are floating, allowing a better grounding configuration. The HV channels give a maximum voltage of 12 kV at maximum current of 1 mA; they can be switched on and off and are fully programmable from remote. The LV channels provide +7 V for the FEB boards at a maximum current of 1 A. They can be switched on and off remotely but are not programmable. All the voltages and currents can be remotely monitored through the communication link driven by the GBs. The communication line is optically decoupled to preserve the floating ground of the voltage channels.

The power distribution represents one the major contributions to the final cost of the RPC system. A possible way to reduce the number of HV channels is to adopt a scheme were the two gaps in a single chamber are powered by different HV lines while the two corresponding gaps belonging to two adjacent chambers in the horizontal (bending) plane share the same HV channel. This configuration would allow to keep a high detection efficiency even in case of failure of a high voltage channel. With this scheme, each DB is able to power two chambers, therefore reducing by a factor of two the number of DBs needed by the system.

3.5.2 Gas system

As stated in Ref. [1] we plan to operate the RPCs with a gas mixture of tetrafluoroethane ($C_2H_2F_4$), isobutane ($i-C_4H_{10}$) and SF_6 in the proportions 95:4:1, a composition tested by us and many groups. The $C_2H_2F_4$ features high density leading to a high primary ionization of about 60 electron-ion pairs per centimeter; the $i-C_4H_{10}$ insures the right amount of quenching, whereas the SF_6 has the purpose to shift the streamer region to larger operating voltages thus widening the plateau [16].

The total gas volume of the RPC chambers is about 1 m^3. The purpose of the gas system

Table 4 Gas specifications for the RPC system.

Gas volume	$\sim$1 m^3
Concentration $C_2H_2F_4$:i$-C_4H_{10}$:SF_6	95:4:1
Concentration accuracy	0.3% absolute
O_2 contamination	$< 1\%$
H_2O contamination	$< 1\%$
Gas overpressure	Max 3 mbar
Purified gas flow rate	0.08 m^3/h
Maximum flow rate	0.64 m^3/h

is to mix the three components to the right proportion and to distribute a clean gas mixture to each individual chamber at a pressure slightly above the atmospheric pressure ($\sim$1 mbar). The hydrostatic pressure differences over the height of the system, measuring vertically about 10 m, are not negligible compared to the required overpressure (the chosen mixture has a hydrostatic gradient of 0.4 mbar/m); the gas distribution system should therefore be able to compensate for these differences.

For RPC systems the gas purity requirements are not very high. The main impurities which may harm the proper functioning of the detectors are oxygen and water vapour. Passed experience with RPCs and studies performed by other groups ([10, 17]) have shown that these contaminations should remain below 1%.

The gas specifications for RPCs are summarized in Table 3.

4 Considerations about construction and assembly

In this section we describe schematically the organization of the production phases, from the bakelite layers to the stockage at CERN.

4.1 Tests of the bakelite layers

The whole amount of bakelite needed for the LHCb RPCs can be produced in one week. A first selection of good plates can be performed directly by the firm by measuring the volume resistivity [4]. The company will also take care of cutting the bakelite plates to the detector dimensions.

A second careful selection of the good plates, looking especially for possible artificial surface roughness of the (melamine) side facing the gas gap, is probably needed and will be done in Rome II. Here the choice of the two plates for a given gap will be also made, which will probably require a new measurement of the resistivity.

4.2 RPC gap production and tests

The industrial capabilities for producing RPC detectors is by now well established, and the whole need of LHCb can be produced in a few months. The gaps will be produced following

[4] The CMS group developed a special tool for a multi-point resistivity measurements [18]; we are investigating the possibility to use the same tool or a similar one specific for our case.

the LHCb specifications, using the same techniques detailed in Refs. [10, 17]. The specifications concern the size of the gaps and of the graphite paint defining the active area; the topology for positioning the spacers; the linseed treatment (if applied). The gap gas thickness and their capability to stand high voltages in Ar or N_2 will also be tested by the producing firm.

The production of the gaps will be closely monitored at the factory by technicians and physicists belonging to the responsible institutes. In the case the oil treatment will be necessary, a procedure has to be defined to control its quality. A possibility would be to perform a routine check by opening up and inspecting a certain fraction of the gas gaps (e.g. one in ten) during the production phase.

4.3 Chamber assembly

Chamber assembly will be done in Rome II and Firenze. The quality of the produced gaps will be checked at first by performing an automated I-V measurement, in parallel to about 10 gaps. For this purpose, the gaps will be equipped with connectors to distribute the high voltage to the graphite layer and to monitor the dark current. The ten gaps will be flushed with gas at a rate of about 3 l/h for about 15 hours; since the gap volume is about 1 liter, this will insure that at least four volumes are changed during the flushing procedure. The tolerances to accept/reject gaps will be defined with the next prototypes. The possibility to use a β radioactive source to check the uniformity of the chambers is under investigation.

Chambers with two good gaps will be equipped with strip planes and closed, and the front-end boards plugged externally as mentioned in Section 3.2.2. At this point the chambers will be ready for the final tests with cosmic rays described in the next section.

The successfully tested chambers will be regularly flushed and measured with cosmic rays until they are shipped to CERN to be installed in LHCb.

4.4 Tests with Cosmic Rays

The final commissioning of the chambers before shipping them to CERN will be performed through a test with cosmic rays. In this test the chambers will be characterised from the point of view of their efficiency, response uniformity, cluster size and time resolution. For this purpose a test station based on a cosmic rays telescope is going to be built in Florence and Rome II.

The parameters of the test station are to a large extent determined by the low cosmic ray rate and by the maximum number of channels that can be reasonably equipped and read out. The station (schematically shown in Figure 19) will consist of a rack where several chambers can be placed under test at the same time. The trigger will consist of two planes of plastic scintillators 2 m long and 60 cm wide, placed above and below the chamber stack. The tracks will be reconstructed with the help of two additional RPCs used as reference chambers. The possibility to accomodate an iron slab at the bottom of the system with the purpose to filter a harder cosmic spectrum, has also been considered.

Given the dimensions of the trigger planes and the cosmic ray rate, a trigger rate of about 50 Hz is expected. In order to test the chamber efficiency as a function of the applied voltage HV, a statistically significant sample of events must be collected for each physical channel and HV value. The strategy to determine the efficiency-HV curve has not been optimized yet. However, with the 6-chamber configuration shown in Figure 19 each physical channel sees a cosmic rate of at least 0.5 Hz. This means that the nine months scheduled for the tests should

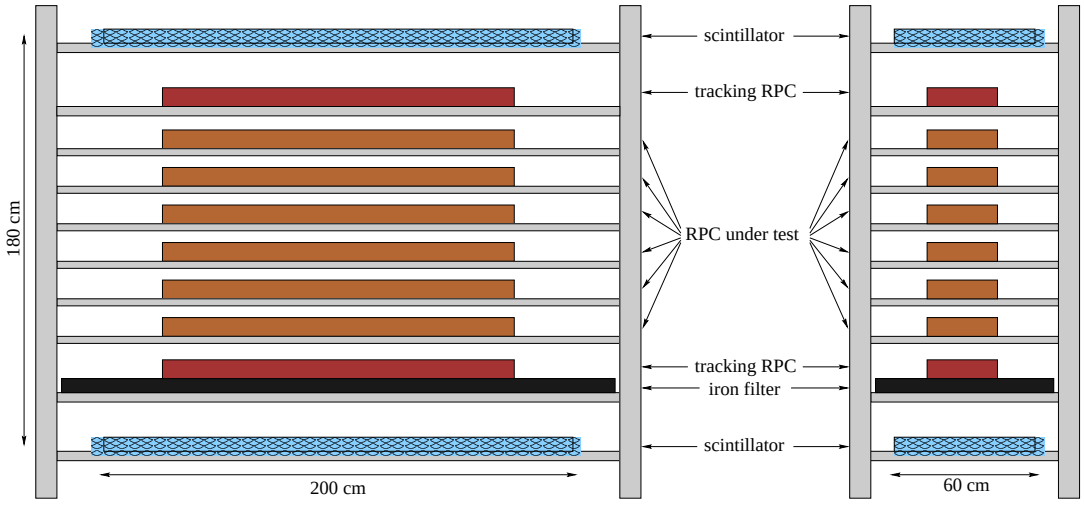

Figure 19 Tests with Cosmic Rays: preliminary setup for a cosmic-ray test station.

allow a sufficiently precise determination of the efficiency-HV curve for each channel of the 480 chambers.

Finally, the test station will have at least 1000 readout channels. As it is unpractical and too expensive to read out all these channels via commercial readout boards (e.g. commercial TDCs and scalers), we have designed and built a dedicated high density pattern-unit board described in the next subsection.

4.4.1 DAQ board for tests

The DAQ board for tests has been specifically developed for testbeam and cosmic rays measurements. The block diagram is shown in Figure 20. The board implements the standard VME 6U protocol and has 64 LVDS input channels. A common gate of programmable width [5] is triggered externally. The number of hits within the gate per input channel are counted by 24-bit scalers. The arrival time for each hit within the gate is measured by 16–bit auto-scale time counters. These functions are provided via a Xilinx FPGA. Up to 512k hits can be stored as 32-bit words in a memory bank. The dead time is less than 100 ns. The board also implements Block–Data–Transfer and JTag protocols.

4.5 Data base

Each chamber/gap will be identified by a bar code which will allow to retrieve all the important facts about the chamber/gap, the history and results of all the measurements done by the companies and in the institute laboratories, and the specification curves.

5 Cost update

The present estimated construction cost for a chamber of approximately 0.3×1.5 m^2 is summarized in Table 5.

[5] Two values, 0.3 and 2.5 s, are preset.

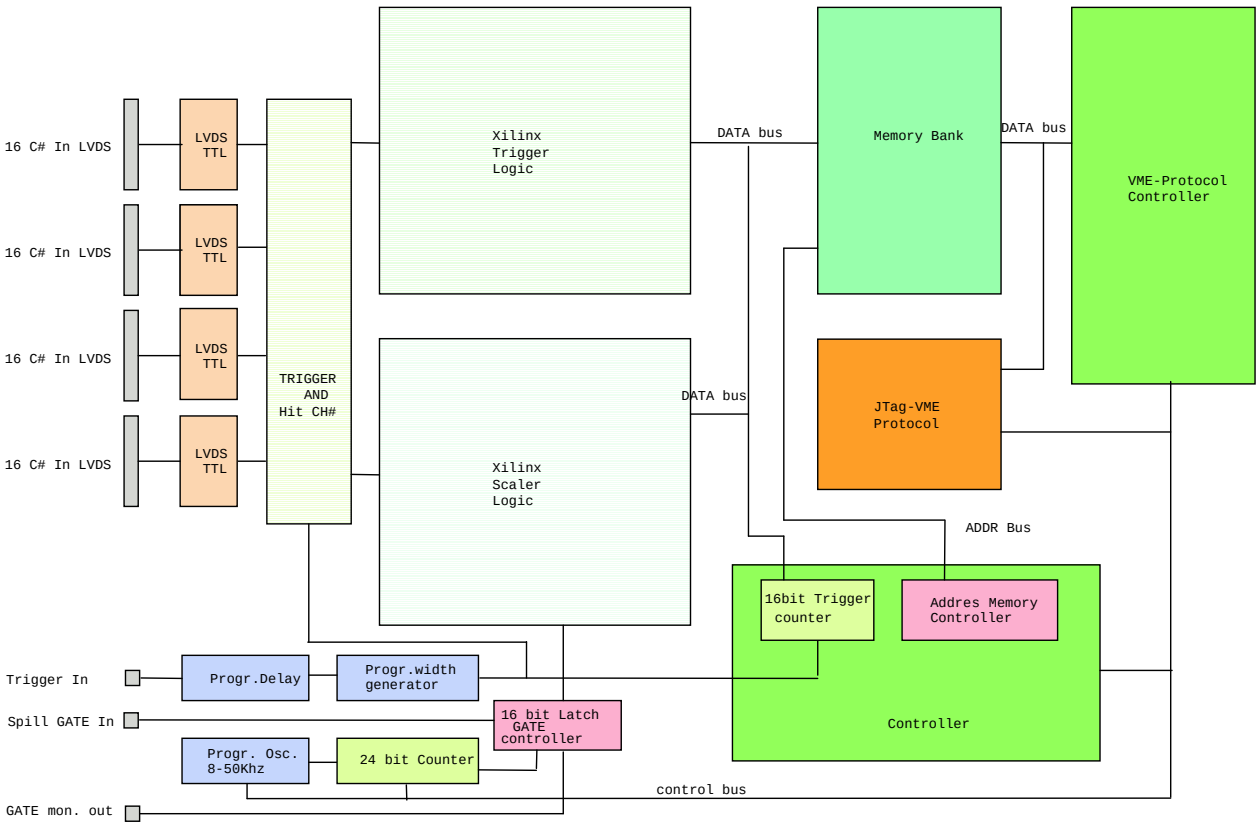

Figure 20 Block diagram for the DAQ board specifically designed for tests.

Table 5 Detail of costs for production of RPC chambers.

Item	Qty. per chamber	Unit cost (CHF)	Cost of chamber (CHF)
Bakelite	2.5 m^2	20	50
Gas gaps production	2	120	240
Strip planes	1 m^2	50	50
Support planes	1 m^2	35	35
HV Connectors	2	12.5	25
Contingency/spares	10 %		40
Mechanics, connectors etc.		50	50
Assembly		50	50
Total			540

The total cost for the 480 chambers foreseen is 260 kCHF including 10% contingency on the individual components.

As far as the front-end electronics is concerned, the bare Bari chip costs about 2.5 CHF per channel to which the cost of the board and of the related components has to be added. Assuming a total 7.5 CHF per channel we end up with about 200 kCHF.

The largest single contribution to final cost will most likely be the HV and LV system. The present estimates indicates that the total cost of this system should not exceed 300 kCHF.

Finally, the estimated cost of the gas system is 160 kCHF.

These estimates must be considered as upper limits.

References

[1] M. Adinolfi et al., “Proposal for the RPC muon detector of LHCb”, LHCb 2000-053.

[2] B. Schmidt et al., “LHCb Muon System by Numbers”, LHCb 2000-089.

[3] LHCb Collaboration, “Muon System Technical Design Report”, CERN LHCC 2001-010, LHCb TDR 4, June 2001.

[4] M. Abbrescia *et al.*, NIM A 456 (2000) 143.

[5] M. Abbrescia *et al.*, in proceedings of the “6^{th} Workshop On Electronic For LHC Experiments”, CERN 2000-010; CERN-LHCC-2000-041.

[6] W. Riegler, “RPC Simulations”, LHCb 2000-112.

[7] A. Kashchuk et al.,”Performance study of a MWPC prototype for the LHCb muon system with the ASDQ chip”, LHCb-2000-062.

[8] D. Moraes et al., “CARIOCA - a fast binary front-end implemented in 0.25 μm CMOS using a Novel current-mode technique for the LHCb muon detector”, LHCb-2000-093.

[9] P. Colrain et al., “Optimization of the Muon System Logical Layout”, LHCb 2000-016.

[10] CMS Collaboration, “Muon Technical Design Report”, CERN LHCC 97-32, CMS TDR 3, December 1997.

[11] J. André et al., ”LHCb Muon Detector support structure and iron filter configuration”, LHCb 2001-031

[12] `http://www.mayahtt.com/tmwiz/default.htm`

[13] See for details: `http://www.pi.infn.it/bfactory/IFR/WorkshopJan2001/program.html` and links therein.

[14] G. Iaselli, Private communication.

[15] A. Lai et al., “LHCb Muon Front-End architecture”, LHCb 2001-030 and references therein.

[16] P. Camarri et al., “Streamer suppression with SF_6 in RPCs operated in avalanche mode”, Nucl. Instrum. Meth. **A** 414 (1998) 317.

[17] ATLAS Collaboration, “Muon Spectrometer Technical Design Report”, CERN LHCC 97-22, ATLAS TDR 10, May 1997.

[18] See for details `http://www.pv.infn.it/~vitulo/cms/cmsnote1.html` and links therein.